Supporting Information

Temperature-Induced Lattice Relaxation of Perovskite Crystal Enhances Optoelectronic Properties and Solar Cell Performance

Banavoth Murali[†], *Emre Yengel*[†], *Wei Peng*[†], *Zhijie Chen*[‡], *Mohd S. Alias*[¶], *Erkki Alarousu*[†] *Boon S. Ooi*[¶], *Victor Burlakov*[§], *Alain Goriely*[§], *Mohamed Eddaoudi*[‡], *Osman M. Bakr*[†], *and Omar F. Mohammed*[†,]*

[†]King Abdullah University of Science and Technology, KAUST Solar Center, Division of Physical Sciences and Engineering, Thuwal 23955-6900, Kingdom of Saudi Arabia,

[‡]King Abdullah University of Science and Technology, Functional Materials Design, Discovery and Development Research Group, Advanced Membranes and Porous Materials Center, Thuwal 23955-6900, Kingdom of Saudi Arabia,

[¶]King Abdullah University of Science and Technology, Photonics Laboratory, Computer, Electrical and Mathematical Sciences and Engineering Division, Thuwal 23955-6900, Kingdom of Saudi Arabia,

[§]Mathematical Institute, University of Oxford, Woodstock Road, Oxford OX2 6GG, United Kingdom

AUTHOR INFORMATION

Corresponding Author

*Email: **omar.abdelsaboor@kaust.edu.sa**

Experimental Section

Chemicals and reagents. In a typical single crystal synthesis, the chemicals and reagents were employed as procured and without further purification. Lead bromide ($PbBr_2$) (≥98%) and dimethylformamide (DMF) (anhydrous, 99.8%) are procured from Sigma-Aldrich and MABr (Methylammonium bromide) purchased from Dyesol Limited (Australia) respectively. Transparent electrode FTO-coated glass substrates (15 Ω sq−1) were purchased from Pilkington.

Synthesis of $MAPbBr_3$ monocrystalline films. Free standing single crystals and monocrystalline thin films were synthesized from $PbBr_2$ (1 M) and MABr (1 M) solutions in DMF prepared at RT reported elsewhere.[1,2] Two pyrex crystallizing dishes A) 80 mm × 40 mm, B) 125 mm × 65 mm were used for the crystallization. The solution mixture is then transferred from a 2 ml filter (0.2-μm pore size) into the dish-A and is then properly sealed by the aluminum foil and Kapton tape. A small aperture of 0.5 mm is made from a syringe onto the sealed foil to allow the diffusion of antisolvent. This dish-A is now slowly placed into the dish-B containing the antisolvent. The whole setup is placed in the dark till the solution reached a low supersaturation state where an ultrasonic pulse in short duration <1s is introduced to trigger the nucleation. The final monocrystalline films/crystals were obtained 3-6 h later following this cavitation-triggered asymmetrical crystallization (CTAC) strategy.

Device fabrication. FTO-coated glass substrates were cleaned using detergent, de-ionized water, acetone, and isopropanol. The electron transporting layer compact TiO_2 layer was spin coated onto the cleaned FTO substrates followed by annealing at 500 °C with a ramping rate of

10°C/min in a muffle box furnace reported elsewhere.[1] Monocrystalline films/crystals were synthesized using the above procedure reported elsewhere.[2] The same geometry masked Au top electrode top is thermally evaporated at a rate of 0.25 Å/s to complete the device architecture Glass/FTO/$MAPbBr_3$/Au. Active device area was measured to be 0.0089 cm^2 the Zeiss optical microscope.

*Measurement and characterization.*Variable Temperature Powder X-ray Diffraction (VT-PXRD) measurements were collected on a PANalytical X'Pert Pro MPD X-ray diffractometer equipped with an Anton-Parr CHC+ variable temperature stage. Measurements were collected at 45 kV, 40 mA for Cu Kα (λ = 1.5418 Å) with a scan speed of 1.0° min^{-1} and a step size of 0.02° in 2 θ. Samples were placed under vacuum during analysis and analysis and the sample was held at the designated temperatures for at least 60 minutes between each scan**.** Cary 6000i spectrophotometer with an integrating sphere using the diffused reflectance accessory (DRA) in the reflectance mode was used to record the steady-state absorption. The cross-sections on the perovskite were performed using FEI Quanta 3DFEG SEM-FIB dual system with Ga^+ ions source, the acceleration voltage of 30 keV, a probe current of 300 pA, dwell time of 1 us and serpentine scanning. SEM cross-sections were performed simultaneously using the same system with a voltage of 5 keV and probe current of 47 pA. Annealing studies were performed at the temperature of 35, 60, 75 and 125 °C, respectively, for 1 hour each using vacuum convection oven. The photoelectron spectroscopy in the air (PESA) was measured using Riken Photoelectron Spectrometer (Model AC-2) by pre-calibrating the UV lamp intensity to 50 nW for measurements. Transient photocurrent measurements are carried out using PAOIS, equipped with white LED source ($2kW/m^2$). Current-Voltage characteristics and photodetection in ambient were demonstrated under A.M. 1.5 G Newport SolAAA, Solar Simulator equipped with Keithley

2400 source measurement unit. The temperature dependent impedance measurements were carried out using a Metrohm Autolab and are simulated using the Nova 1.11 software. Time-correlated single photon counting (TCSPC) measurements were performed by using a Halcyone spectrometer (Ultrafast Systems, LLC) and a femtosecond laser source. During the measurements, samples were suspended in a cuvette filled with 1,2-dichlorobenzene (DCB) and excited with laser pulses at 800 nm with 1 kHz repetition rate and 35 fs pulse duration. Temperature controlled cuvette holder (FLASH 300, Quantum Northwest) is employed for the temperature dependent lifetime measurements. The solution is stirred at a constant rate during the measurements to maintain the temperature stability.

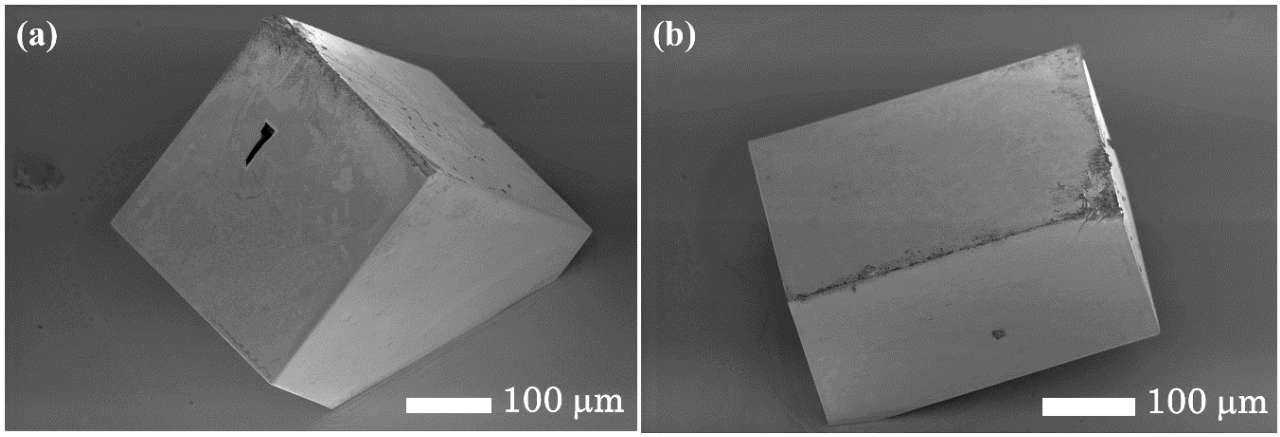

Figure S1. (a, b) SEM images showing two freestanding single crystals obtained from the CTAC method.

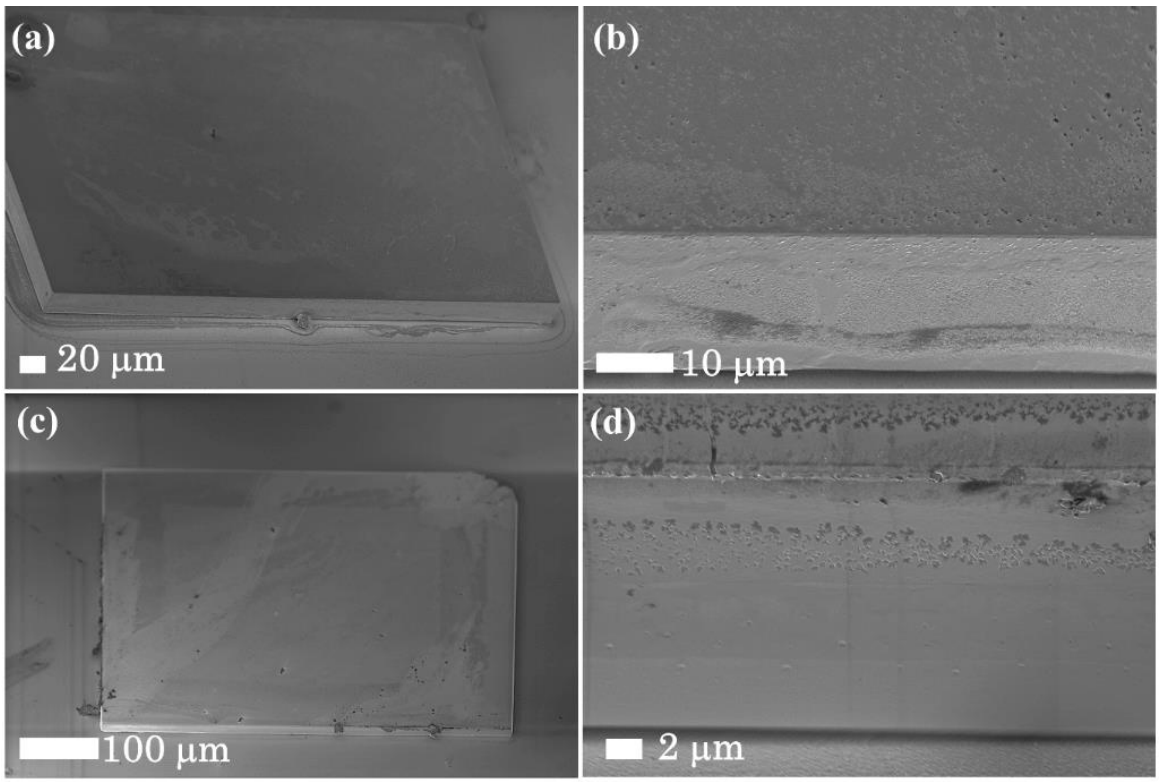

Figure S2. (a-d) SEM images showing various thicknesses of monocrystalline thin films obtained by CTAC method.

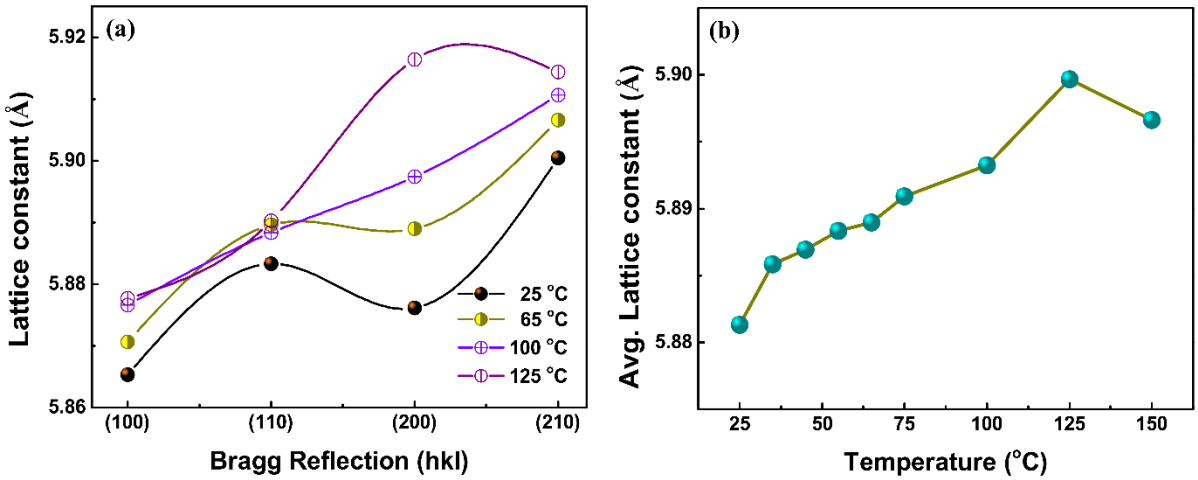

Figure S3. a) Variation of lattice parameter with respect to each Bragg reflection and b) average lattice constant as a function of temperature respectively.

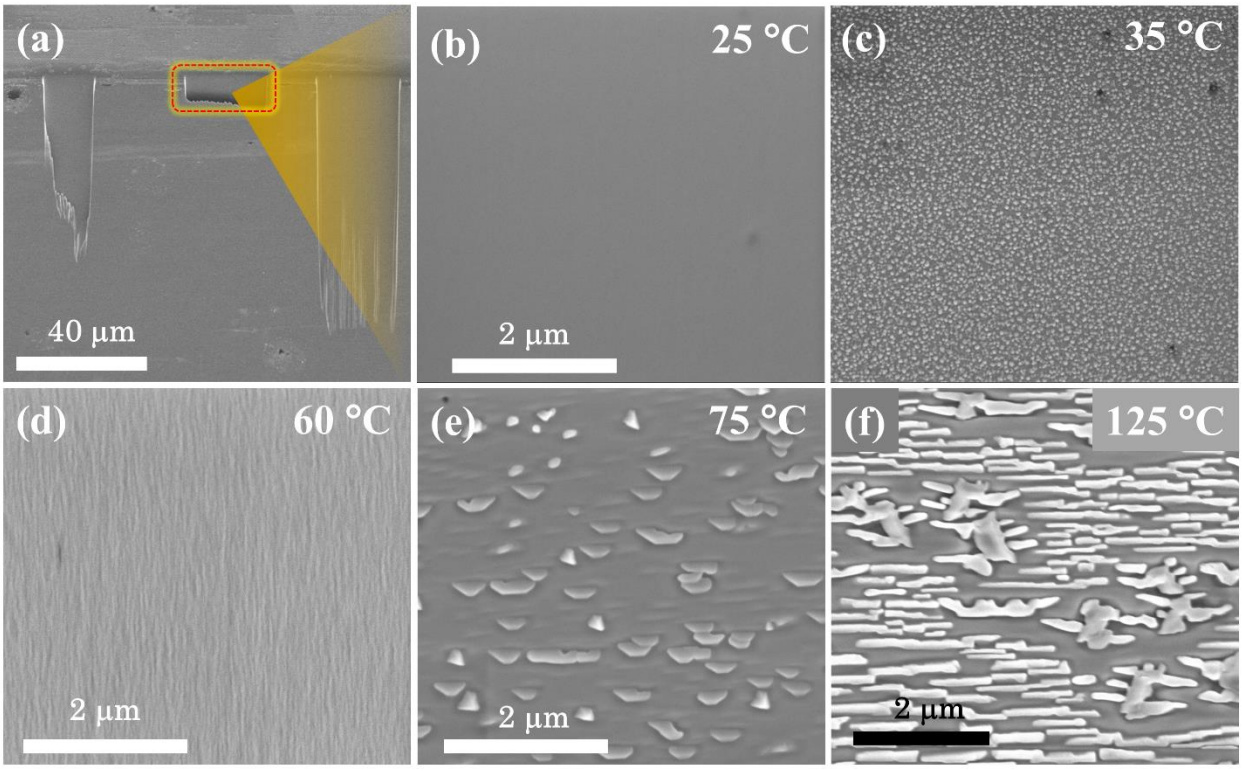

Figure S4. (a-f) FIB SEM micrographs of a $MAPbBr_3$ single crystal at various temperatures as indicated in each figure panel.

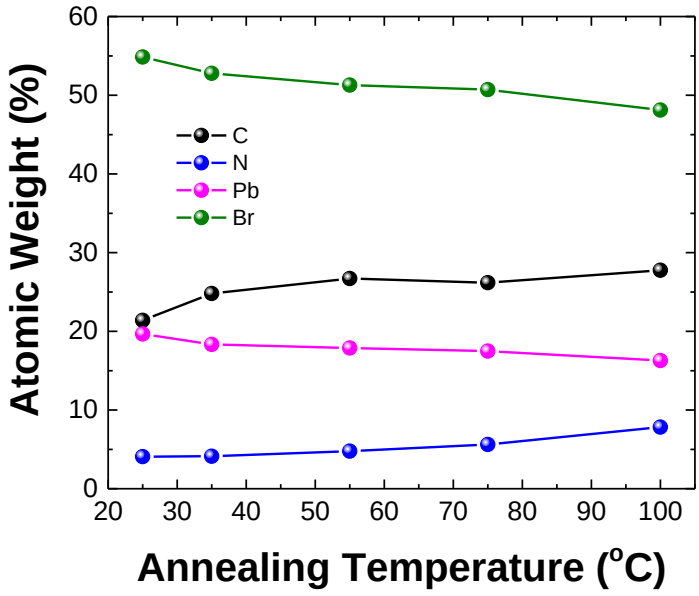

Figure S5. Compositional analysis performed at various annealing temperatures on $MAPbBr_3$ single crystal.

The optical absorption, which is the key functionality to realize optoelectronic devices, showed a clear band cutoff with no absorption tails or exciton signatures when subjected to annealing, further corroborating the thermal stability and preserved crystallinity (Figure S6a). A slight shift in the bandgap was noted (from 2.179 eV at 25 °C to 2.171 eV at 150 °C), as estimated from Tauc plots, assuming that the direct parabolic bands were near the band edges (Figure S6b). To further substantiate the impact of annealing, comparative band energy levels were constructed from the work functions corresponding to the highest occupied molecular orbital (HOMO) levels by performing photoelectron spectroscopy in air (PESA) (Figure S7, Figure S8) and UV-Vis optical bandgap measurements on a free-standing $MAPbBr_3$ single crystal. The electronic level results corroborate those of XRD, and thus, this anomalous trend is attributable to the relaxed cubic lattice in the aforementioned window and to the strained system at the other two extremities (25 °C and 125 °C).

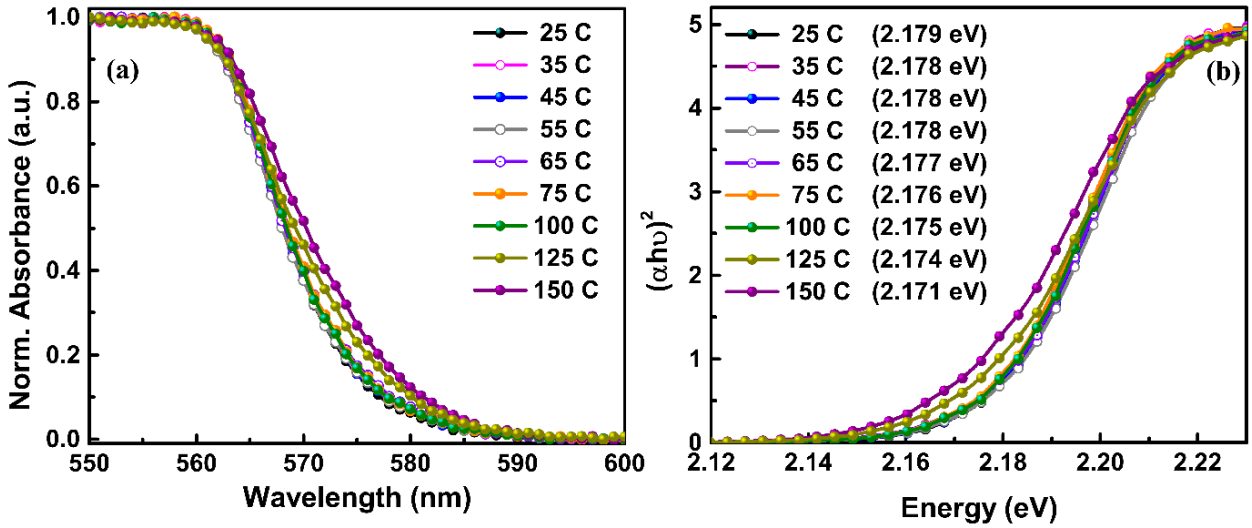

Figure S6. a) Steady state absorbance of $MAPbBr_3$ and b) Tauc plot estimating the energy band gaps for various temperatures.

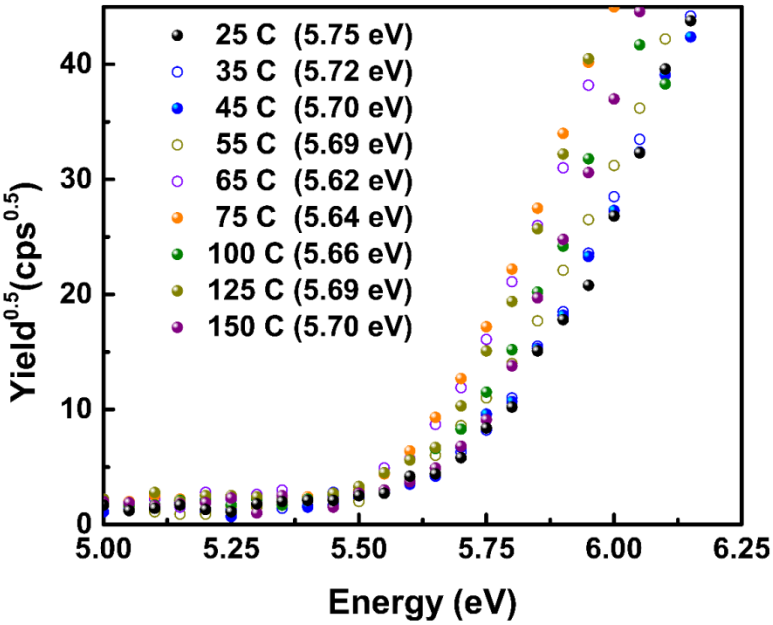

Figure S7. Photoelectron spectroscopy in air (PESA) measurements estimating the HOMO levels for various temperature annealed $MAPbBr_3$ freestanding single crystals.

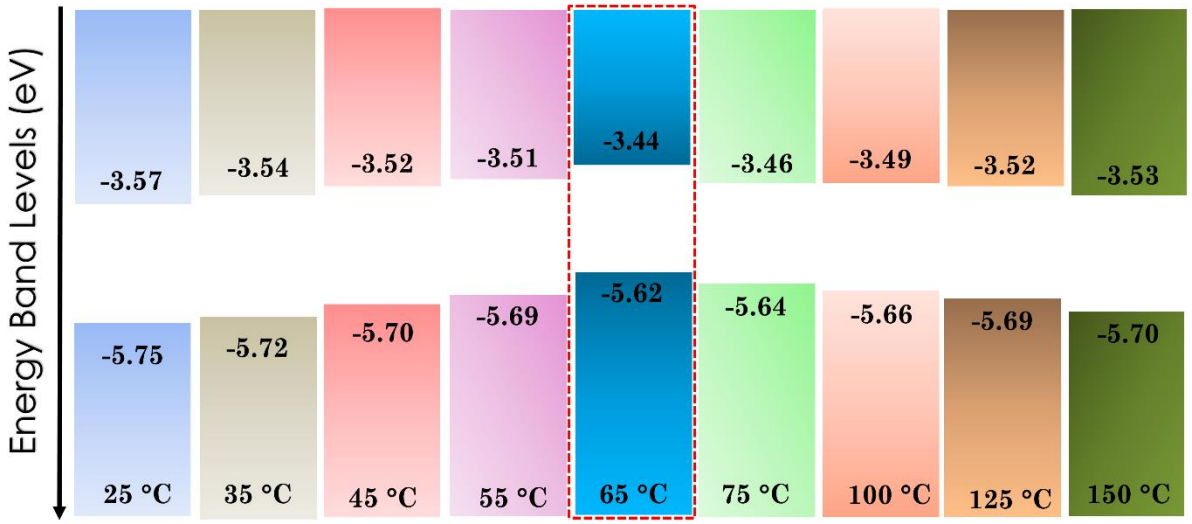

Figure S8. Schematic energy level diagram estimated from the Tauc plot and the PESA measurements for various temperature annealed $MAPbBr_3$ freestanding single crystals.

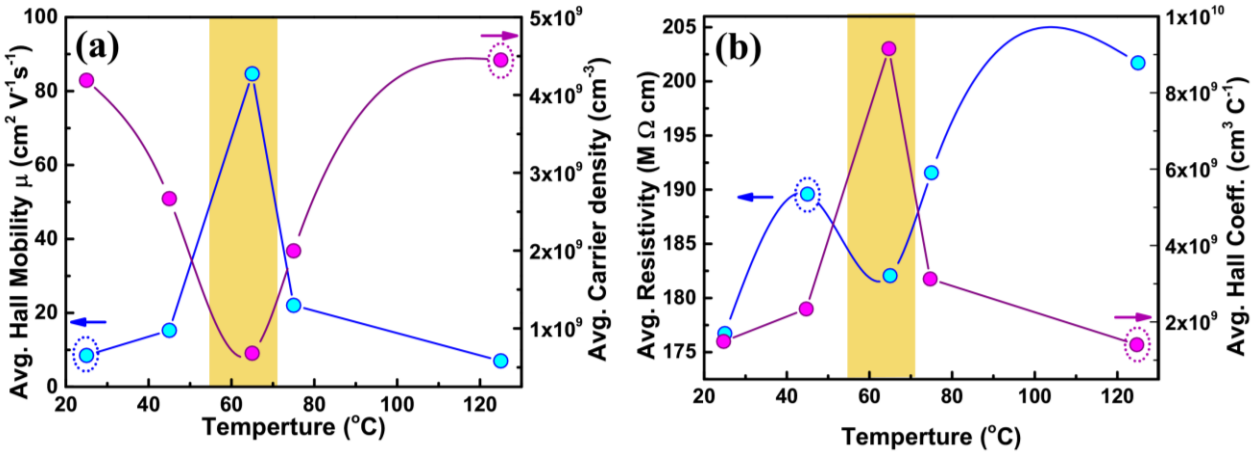

Figure S9. Variation of Hall measurement parameters such as a) avg. Hall mobility (left panel), and avg. carrier density (right panel), b) avg. resistivity (left panel), Hall coefficient (right panel) as a function of temperature.

Similarly, various models were used in case of $MAPbI_3$ to understand the recombination and carrier dynamics using TRPL.[3] The long temperature dependent PL decay[4] lifetimes indicate the changes in the electronic structure and excited-state dynamics at different temperatures. The time evolution of the concentration of photo-excited electron where $\tau = \left(\gamma \cdot n_e(0)\right)^{-1}$ expressing the characteristic PL decay time with its temperature dependence, is shown in Figure 5 (a-c). According to the lifetimes determined at high temperatures, clearly, the temperature-dependent recombination lifetimes behave similarly to the electrical properties. By contrast, increasing the temperature above 70 °C decreased the charge carrier lifetime. Because the organic cations in the perovskite network can act as rattling centers,[5] the residual strains (tensile or compressive) in the insets of Figures 5a and 5c, which were applied to those cations, can form trap states and engendering a dislocation in the lattice. As the lattice strain is minimized as shown in the inset of Figure 5b, the perovskite lattice assumes a relaxed form, minimizing these dislocations.

According to this model[6] the time evolution of the concentration of photo-excited electrons n_e (holes $n_h = n_e + n_{h0}$) is described as Eqn. S1.

$$\frac{dn_e}{dt} = -\gamma \cdot n_e \cdot \left(n_e + n_{h0}\right) \tag{S1}$$

where γ is recombination constant, which includes both radiative and non-radiative direct and trap-assisted recombination processes. The parameter n_{h0} accounts for background hole concentration. Using the solution to this equation, we obtain an expression (Eqn. S2) for time-dependent PL intensity

$$I_{PL}\left(t\right) = P_3 \cdot \frac{\exp\left(-P_1 \cdot t\right)}{\left(1 + P_2 \cdot \left(1 - \exp\left(-P_1 \cdot t\right)\right)\right)^2} + P_4 \tag{S2}$$

where the two parameters of interest are $P_1 = \gamma \cdot n_{h0}$ and $P_2 = n_e\left(0\right) / n_{h0}$, which values obtained by fitting experimental data with function given by Eqn. S2 are given in Figure 5 (a-c). Here $n_e\left(0\right)$ is the electronic concentration at t=0 after the laser pulse. The parameters P_3 and P_4 take into account the uncertainties in the scaling and background level of the instrument. Note that Eqn. S2 describes both the monomolecular ($n_e\left(0\right) << n_{h0}$) and bimolecular ($n_e\left(0\right) >> n_{h0}$) recombination and all the intermediate regimes. The value $\tau = \left(\gamma \cdot n_e\left(0\right)\right)^{-1}$ has a meaning of the characteristic PL decay time. Its temperature dependence is shown in the inset of Figure 5c. Therefore from the modeling of the experimental TRPL, longer carrier decay time indicate a probable enhancement of device performance at 60 °C compared to other temperatures. Thus, the effective carrier collection is expected to increase because of the comparatively longer carrier lifetimes.

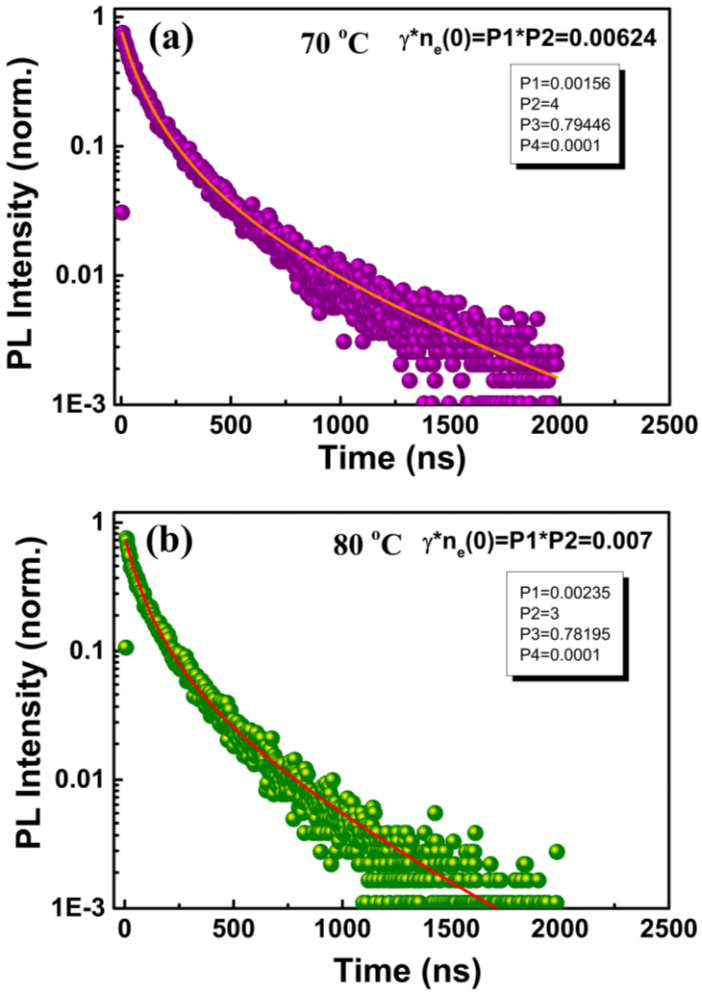

Figure S10. (a, b) Time-resolved PL lifetimes measured on $MAPbBr_3$ single crystal at 70 °C and 80 °C respectively.

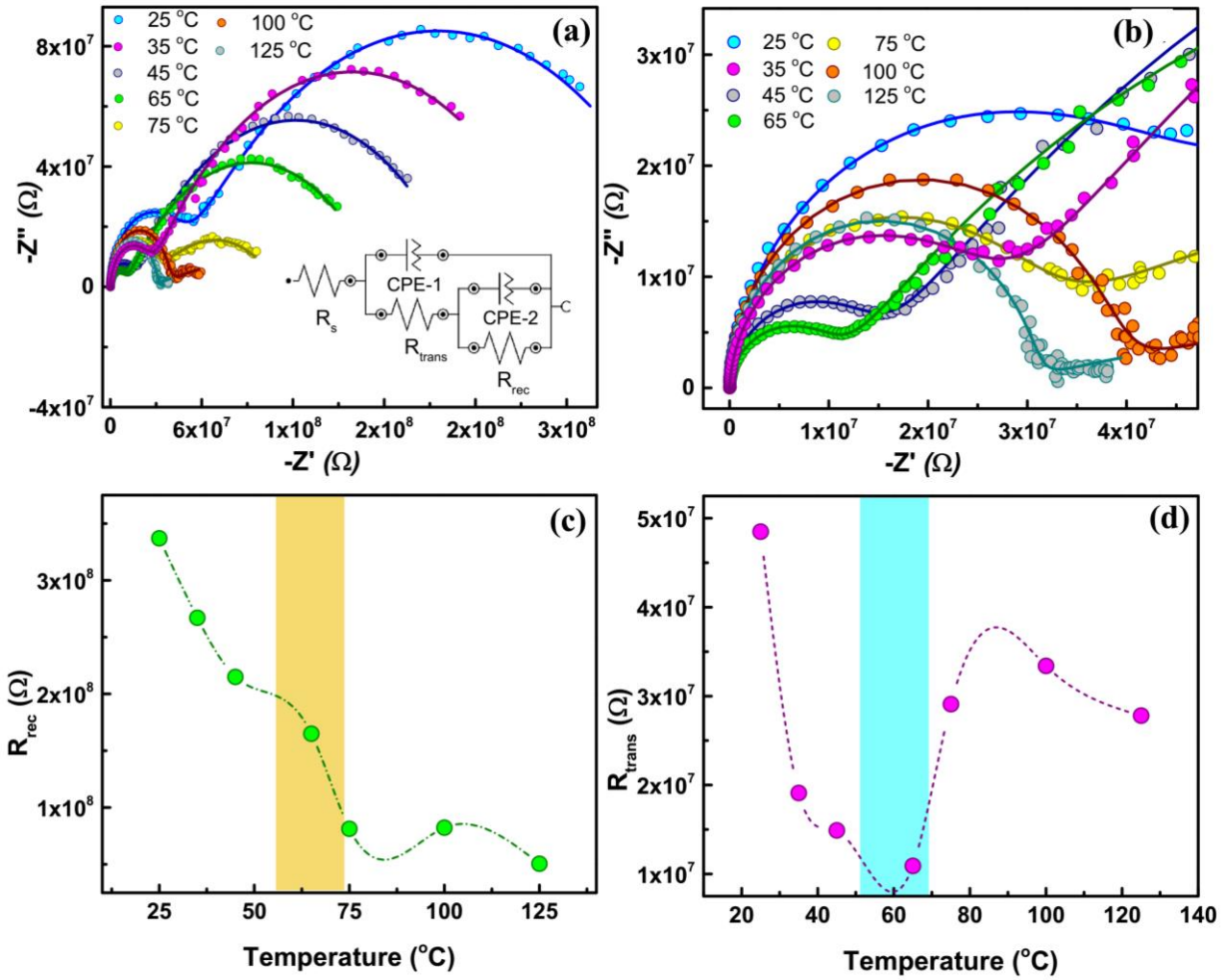

Figure S11. (a, b) Complex Impedance Nyquist plots with the equivalent circuit in the inset. (c, d) Recombination and transport resistances as a function of temperature.

REFERENCES:

1. Peng, W.; Wang, L. F.; Murali, B.; Ho, K. T.; Bera, A.; Cho, N.; Kang, C. F.; Burlakov, V. M.; Pan, J.; Sinatra, L.; et al. Solution-Grown Monocrystalline Hybrid Perovskite Films for Hole-Transporter-Free Solar Cells. *Adv. Mater.* **2016,** *28*, 3383-3390.
2. Shi, D.; Adinolfi, V.; Comin, R.; Yuan, M.; Alarousu, E.; Buin, A.; Chen, Y.; Hoogland, S.; Rothenberger, A.; Katsiev, K.; et al. Low trap-state density and long carrier diffusion in organolead trihalide perovskite single crystals. *Science* **2015,** *347*, 519-522.

(3) Yamada, Y.; Nakamura, T.; Endo, M.; Wakamiya, A.; Kanemitsu, Y. Photocarrier Recombination Dynamics in Perovskite $CH_3NH_3PbI_3$ for Solar Cell Applications. *J. Am. Chem. Soc.* **2014,** *136*, 11610-11613.

(4) Yamada, T.; Yamada, Y.; Nishimura, H.; Nakaike, Y.; Wakamiya, A.; Murata, Y.; Kanemitsu, Y. Fast Free-Carrier Diffusion in $CH_3NH_3PbBr_3$ Single Crystals Revealed by Time-Resolved One- and Two-Photon Excitation Photoluminescence Spectroscopy. *Adv. Electron. Mater.* **2016,** *2*, 1500290.

(5) He, Y. P.; Galli, G. Perovskites for Solar Thermoelectric Applications: A First Principle Study of $CH_3NH_3Al_3$ (A = Pb and Sn). *Chem. Mater.* **2014,** *26*, 5394-5400.

(6) Zhang, W.; Pathak, S.; Sakai, N.; Stergiopoulos, T.; Nayak, P. K.; Noel, N. K.; Haghighirad, A. A.; Burlakov, V. M.; deQuilettes, D. W.; Sadhanala, A.; et al. Enhanced Optoelectronic Quality of Perovskite Thin Films with Hypophosphorous Acid for Planar Heterojunction Solar Cells. *Nat. Commun.* **2015,** *6*, 10030.